Graphical Abstract

In situ measurement of friction on the human body

Pearson A. Wyder-Hodge,Egor Larionov,Dinesh K. Pai

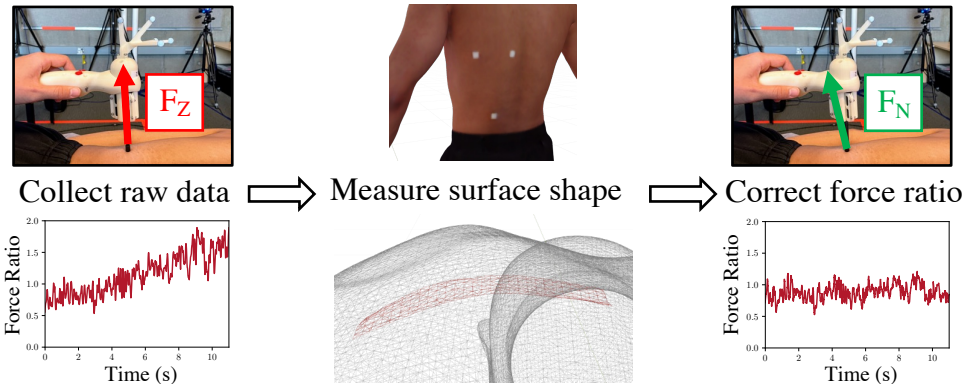

Highlights

In situ measurement of friction on the human body

Pearson A. Wyder-Hodge,Egor Larionov,Dinesh K. Pai

- Implement a curved surface correction method in 3D with a linear sliding handheld tribometer.
- Test methods for capturing the 3D curved surface shape for the surface correction method
- Measure sliding friction on a human body

In situ measurement of friction on the human body

Pearson A. Wyder-Hodge[a,*], Egor Larionov[a] and Dinesh K. Pai[a,b]

[a] University of British Columbia, 2329 West Mall, Vancouver, BC Canada V6T 1Z4
[b] Vital Mechanics Research, Vancouver, BC Canada

ARTICLE INFO

Keywords:
Friction
Measurement
Sliding
Topography

ABSTRACT

Measuring friction on the human body is challenging on areas where the surface of the skin is curved. Handheld devices for measuring friction may make it easier to rapidly measure from hard-to-reach areas, however, the orientation of the probe relative to the surface is often sub-optimal to reliably measure the normal force.

Here, the friction on the surfaces of a mannequin and a human body are measured and corrected using a curvature correction technique. This is accomplished by accounting for the shape of the measurement surface and the orientation of the measurement device relative to that surface. Two strategies for constructing the surface shape of the measurement surface are compared.

1. Introduction

Accurately and reliably measuring friction between the skin on human bodies and other surfaces is important for basic research and many industrial applications. In the textile and fashion industry, it is critical to consider the relationship of friction to the tactile sensation and comfort of the garments [1, 2, 3, 4, 5]. In sports, optimizing the friction between skin and garments or wearable equipment can minimize the risk of injury due to blisters or abrasions, and improve performance [6, 7]. Too much friction between the skin and personal protective equipment may lead to abrasion and discomfort [8].

Many factors need to be considered when measuring skin friction because the results depend on variables such as anatomical location, moisture content, material properties of the skin, and the counter surface [9]. Furthermore, the human body is curved and each body has a unique shape and size, which makes it imperative to consider the surface geometry during measurements. If the surface shape is not considered, then errors during data collection may occur. Often in skin friction research, the force coordinate frame of a tribometer is fixed and the normal force (f_N) is reported as the tribometer's force vector perpendicular to the surface plane at the contact point of the tribometer (f_z for the tribometer used in this research). f_N is defined as the surface force exerted in the perpendicular direction between two contacting surfaces. Therefore, if the force measurement reported by the tribometer is truly the f_N, then that requires the f_z to be aligned with the contact point surface normal during the entire sliding contact. It is unreasonable to expect that a human operating a handheld tribometer can accomplish this alignment (see Fig. 1). Even linear sliding motorized arm systems that are not human-operated, often rely on the surface being flat. This limitation may partially explain why many measurements of skin friction have been conducted on less curved areas of the body, such as the forearm (in addition to the limbs being easier to stage in motorized tribometer setups).

Measuring skin friction at different anatomical locations is often conducted with a tribometer that rotates with the axis of rotation perpendicular to the skin [10, 11, 12, 13]. These tribometers mitigate the surface shape problem by being held statically on the measurement location. Nevertheless, there are disadvantages to these devices, such as being less representative of the sliding contacts that are more common in everyday life and transient changes to the skin due to

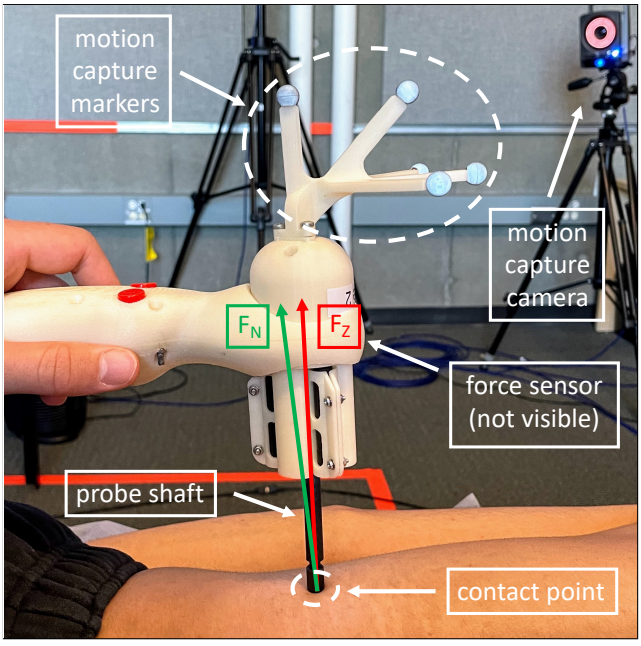

Figure 1: The handheld tribometer makes contact with the skin on the back of a human participant at the end of the probe shaft. The other end of the probe shaft is attached to a 6-DOF force/torque sensor housed within the probe. The motion capture cameras track the position of the motion capture markers attached to the tribometer. The f_N and the f_z are pictured here to display the misalignment between these vectors.

*Corresponding author
ORCID(s):

occlusion of the skin [9]. Research regarding sliding friction on multiple areas of the body has been conducted and has shown differences in the coefficient of friction (COF) at different anatomical locations [14, 5]. However, it is unclear how or if the curved nature of the measurement locations was taken into account in this research.

Wyder-Hodge et al. [15] demonstrated that if the surface shapes, locations, and force sensor orientations are known, then it is possible to estimate the f_N and tangential forces (f_T), regardless of the orientation of the probe to the surface. This was shown to work well in 2D on simple analytically defined curves and skin-like silicone surfaces. Here, this method is applied in 3D on the more complex surfaces of a mannequin and a human participant. On the mannequin, friction is measured at two locations with three different surface materials attached to the surface. On the human participant, the measurement is taken on the skin directly at three different locations. Two strategies for obtaining the surface shapes of the measurement targets are used: a 3D body scanner and a surface mesh generated from a 3D point cloud from motion capture data collected from the tribometer. Furthermore, it is demonstrated that the surface normal on a 3D mesh can be easily estimated using free off-the-shelf 3D geometry processing libraries for this application.

2. Methods

This section outlines the details of the tools and methodology used in the proposed experiments.

2.1. Skin probe

The tribometer is a skin measurement probe, shown in Fig. 1, that has been custom designed to track the position, rotation, and forces at the probe tip contact frame [16]. Motion capture markers are attached to the probe and tracked by an optical motion capture system (Vicon, Oxford, UK). As well, markers are attached to the measurement target to track the relative position and orientation between the target and the tribometer. The skin probe contains a force-torque sensor with six degrees of freedom (F/T Nano 17, ATI Industrial Automation, USA). The sensor is attached to a stiff carbon fiber shaft. The probe housing is 3D printed with Polylactic Acid (Ultimaker 3, Netherlands). The lightweight plastic housing introduces flexion in the probe's structure and a direction-dependent force bias. Through calibration [15], the force bias is accounted for and the forces measured at the force sensor frame are transformed to the probe tip frame, producing the calibrated force, $\boldsymbol{f} = (f_x, f_y, f_z)$.

2.2. 3D surface mesh collection

Two strategies were implemented to collect 3D digital surface meshes of the measurement targets.

The first method uses a 3D full body scanner (VITUS 3D Body Scanner, Human Solutions, Germany). In this paper, this scanner is referred to as the extrinsic scanner, since it is external to the tribometer device. The extrinsic scanner is a large rectangular box designed to capture a high-resolution point cloud (approximately 300 points/cm^2) representing a human in a canonical upright standing position. The point cloud is then converted to a 3D surface mesh using the Anthroscan software package (Human Solutions, Germany). To determine the location of the motion capture markers in the scan, white double-sided tape cut into squares (1 cm x 1 cm) are attached to the body in the corresponding locations for the scan. By identifying these locations on the mesh, the surface mesh can be registered to the motion capture data.

The second method involves scanning a point cloud around the measurement location using the tribometer itself. Since the tip of the skin probe is already being tracked with the motion capture system, it is a simple method to implement before the friction measurements. At each measurement location, the probe tip is traced around the path where the friction measurement was collected. This point cloud is then used to generate a smooth surface mesh using the

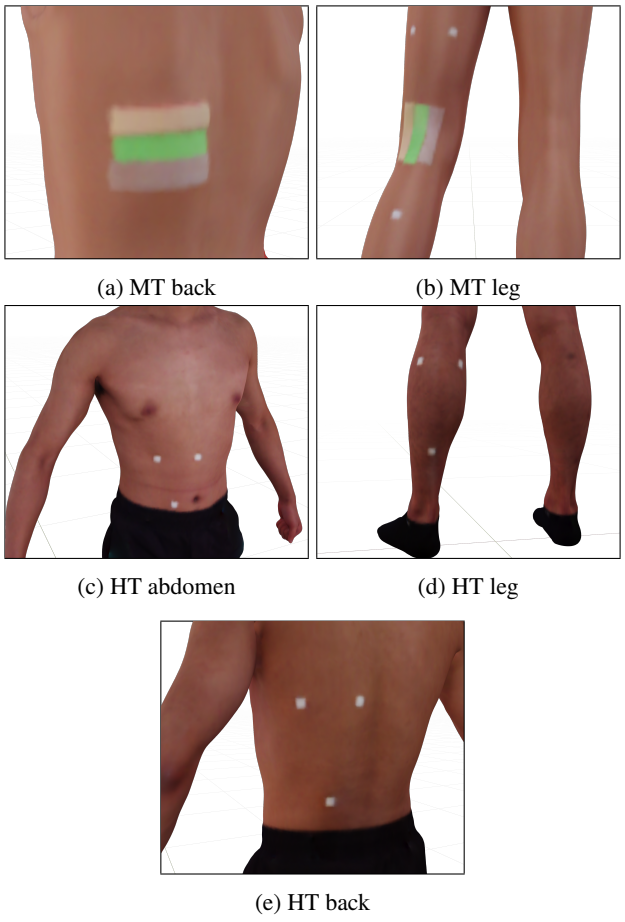

(a) MT back (b) MT leg

(c) HT abdomen (d) HT leg

(e) HT back

Figure 2: Measurement locations for the MT and HT. The images are of the extrinsic scan results. Fig. 2a and Fig. 2b display the back and leg measurements of the MT, respectively. The 3 surface material variables are displayed, from top to bottom in Fig. 2a: silicone, lycra, and polystyrene. Fig. 2c, Fig. 2d, and Fig. 2e display the abdomen, leg, and back measurement locations on the HT, respectively. The white markings around the measurement locations are the pieces of tape used to landmark where the motion capture markers will be placed.

Poisson surface reconstruction method [17] implemented by the Open3D python library [18]. This method is referred to as intrinsic scanning because it uses the probe itself to generate the surface mesh.

The extrinsic scanner has advantages over the intrinsic scanner, such as speed and accuracy. For instance, the extrinsic scanner can collect a full point cloud of an entire human body with a density of approximately 300 points/cm^2 in 10 seconds. As well, the reconstruction of the point cloud creates a smooth surface. However, one issue with this strategy is that the surface of the body will often change shape between the extrinsic scanner capture and the friction measurements because the participant must move from the extrinsic scanner to the motion capture volume. This can cause errors in the surface correction pipeline if the shape of the measurement surface is significantly different due to the positioning of the participant. This error can be mitigated by placing the motion capture markers around the measurement locations on one rigid body segment (e.g. lower leg). Nevertheless, even changes in muscle activation can change the surface shape of the body segment. Areas such as the shoulder, where the rotation of the joint is complicated and involves many different structures, can introduce a lot of variability with very small changes to the position of the participant.

An advantage of the intrinsic scanning technique is that the participant is not required to move places between the intrinsic scanning and friction measurements. Therefore, it is less likely that the surface shape will change between the scanning and measurement phases. Furthermore, this technique does not require an extrinsic scanner, which is expensive monetarily and space-wise in a laboratory. Nevertheless, scanning the skin surface using the probe causes the skin to deform, which can produce inconsistent and inaccurate surface scans. Human skin and the underlying tissue are soft, so the experimenter must maintain a very light touch to avoid excessive deformation, while continuously maintaining contact with the skin. Otherwise unwanted artifacts may be introduced to the resulting point cloud. Likely due to these errors, it was found that the optimal strategy for collecting point cloud data was tracing around the probing location once, rather than collecting many points along the measurement surface (e.g. many linear slides along and adjacent to the measurement path). Too many points included during intrinsic scanning would often result in unwanted roughness and noise due to overfitting in the meshing software. Since the extrinsic scanner does not make contact with the measurement target, it is not vulnerable to these types of errors.

2.3. Measurement

A typical measurement protocol, which was used in the experiments reported in Section 2.5, is briefly summarized here. Motion capture markers are attached to the measurement targets at the locations where the white tape is applied before the extrinsic scan. The positions of the markers on the target and the skin probe are tracked during the friction measurements. The probe tip surface is cleaned with isopropyl alcohol and air-dried for 10 minutes before the measurements. For each location, the experimenter aims to apply a force f_z of approximately 0.5 N. Precise control of the force is not necessary. Five sliding friction measurements were conducted at each location on both targets.

2.4. Surface correction

f_T and f_N are estimated using a surface correction strategy introduced in Wyder-Hodge et al. [15]. Given the force vector $\boldsymbol{f}$ in the probe tip frame, it is sufficient to apply a change of basis to find the same force $\boldsymbol{f}^{\text{adj}}$ expressed in the contact frame:

$$\boldsymbol{f}^{\text{adj}} = R\boldsymbol{f} \tag{1}$$

where R is a change of basis matrix.

The surface mesh of the measurement patch is registered to the motion capture of the target. This orients the patch into the same frame as the captured probe tip locations. The registration is done for each trial individually to control for any movement of the measurement targets. The vector normal to the surface at the point of contact, $\hat{\boldsymbol{n}}$, can be calculated at each face of the 3D surface mesh that the tribometer's path is registered to [19]. With $\hat{\boldsymbol{n}}$ and the orientation of the probe tip, $\hat{\boldsymbol{t}}$, R can be computed using Rodrigues' formula:

$$R = I + \sin\alpha[\hat{\mathbf{k}}]_\times + (1-\cos\alpha)[\hat{\mathbf{k}}]_\times^2$$

where $\cos\alpha = \hat{\boldsymbol{t}}\cdot\hat{\boldsymbol{n}}$, I is the 3×3 identity, $\hat{\mathbf{k}} = \hat{\boldsymbol{t}}\times\hat{\boldsymbol{n}}/|\hat{\boldsymbol{t}}\times\hat{\boldsymbol{n}}|$ and $[\cdot]_\times$ is the cross product matrix:

$$[\mathbf{k}]_\times = \begin{bmatrix} 0 & -k_z & k_y \\ k_z & 0 & -k_x \\ -k_y & k_x & 0 \end{bmatrix}.$$

Because $\boldsymbol{f}^{\text{adj}}$ is in the contact point frame, the normal and tangential force magnitudes can be defined by

$$f_N = f_z^{\text{adj}}$$
$$f_T = \|(f_x^{\text{adj}}, f_y^{\text{adj}})\|.$$

Three friction ratios are computed for each sliding contact for comparison in this study. The raw force ratio is defined as

$$r = f_{xy}/f_z$$

and the corrected force ratio is given by

$$r_c = f_T/f_N.$$

One r_c is calculated for each of the two surface meshes corresponding to each measurement location (see Section 2.4). r_{cb} and r_{cp} are defined as the r_c produced using the surface mesh from the extrinsic scanner and the intrinsic scanner, respectively.

2.5. Experiments

The proposed method for sliding friction measurement was tested on two measurement targets. The first target was a male-fit mannequin. Two locations were measured on the mannequin target (MT):

- the inferior scapular region of the back (Fig. 2a)
- the posterior region of the knee (Fig. 2b).

These locations were chosen to test the robustness of the surface correction, as the scapula location is a convex shape and the posterior portion of the knee is a concave shape. Three materials were cut into strips and attached in a relaxed state with double-sided tape to each of the measurement locations on the MT. The materials included skin-like silicone, lycra fabric (90% polyester and 10% spandex), and flexible polystyrene. The surfaces on the MT were carefully wiped with a dry cloth to remove any dust.

The second measurement target was a 22-year-old male student who provided written informed consent. The measurement locations on the human target were not altered as to measure the skin in its natural condition. Three locations on the human target (HT) were identified for measurement:

- the lateral abdomen (Fig. 2c),
- along the skin where the posterior portion of the tenth rib projects (Fig. 2e), and
- the medial posterior portion of the lower leg (Fig. 2d).

The selected locations were based on their infrequent use in skin tribology research, in contrast to more accessible areas such as the forearm and hand. Additionally, these locations varied in their degree of curvature, with the lower leg being the most curved.

3. Results and Discussion

3.1. 3D surface mesh

3D surface meshes were generated with the two scanning strategies. The surface meshes generated from the extrinsic scanner are shown in Fig. 2 for both of the measurement targets. The scans displayed are reconstructed from the point clouds collected with the extrinsic scanner. The white squares on the scan mark the locations for motion capture registration.

The intrinsic scanning method produced surface meshes for each measurement location. Fig. 3a displays a meshing result from the intrinsic scanning method for the silicone patch on the back measurement location of the MT. This surface mesh is overlaid on the extrinsic scan result for comparison.

Fig. 3b shows the tip path registered for one sliding trial on the back measurement location of the MT. The tip position for every measurement is registered to both the extrinsic scanner mesh and intrinsic scanner mesh and the surface normal at each contact point is calculated for the force correction. The mean difference of the normals

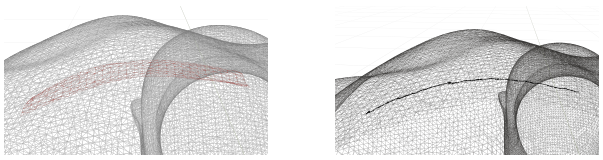

(a) (b)

Figure 3: Fig. 3a displays a mesh generated from the intrinsic scanning technique (red) and the mesh generated from the extrinsic scanner (grey) at the same location for comparison. Fig. 3b shows the registered tip position (black) of a measurement on the extrinsic scan (grey) of the MT

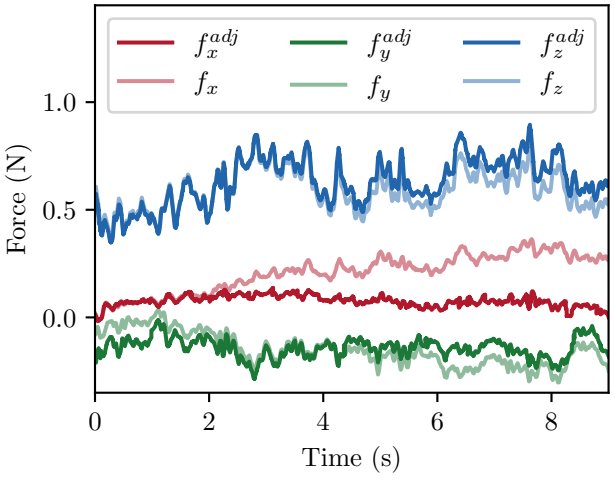

(a)

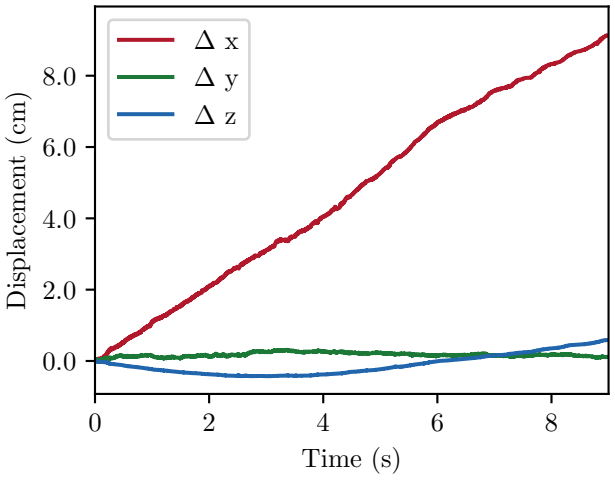

(b)

Figure 4: Force and displacement data for one sliding trial for the lycra condition at the leg measurement location on the MT. Fig. 4a shows the raw forces (f_x, f_y, f_z) and adjusted forces ($f_x^{adj}, f_y^{adj}, f_z^{adj}$). Fig. 4b shows the displacement of the probe tip position in the motion capture world frame.

calculated for each of the surface meshes on the same sliding measurements is 6.98°. This number is supported qualitatively by observing that the intrinsic scanning meshes often

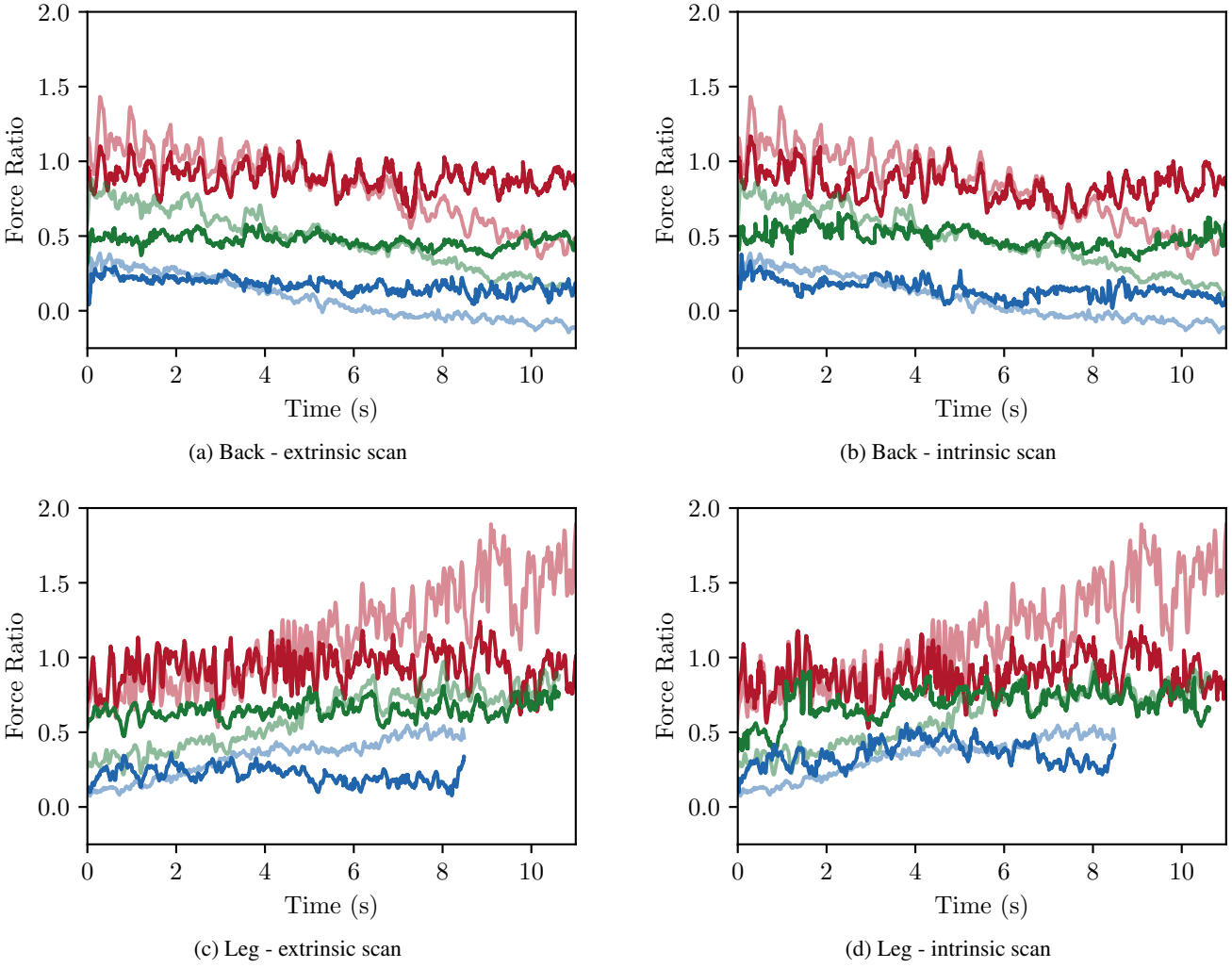

(a) Back - extrinsic scan

(b) Back - intrinsic scan

(c) Leg - extrinsic scan

(d) Leg - intrinsic scan

Figure 5: MT results on the back and leg measurement locations. Red is the silicone surface, green is the polystyrene surface, and blue is the lycra surface. The translucent traces represent r. The opaque traces in Fig. 5a and Fig. 5c represent r_{cb}. The opaque traces in Fig. 5b and Fig. 5d represent r_{cp}. Each line corresponds to a single touch across the surface.

produced a noisier and rougher surface than the extrinsic scanning meshes.

The experiments confirmed the tradeoffs discussed in Section 2.2 between the use of an extrinsic scanner and intrinsic scanning using the mobile probe. Taken together, the results suggest that if an extrinsic scanner is available, it is advantageous to use it on stiffer body segments or to save the experimenter and participant time if there are many areas to measure. However, for areas where the body surface shape changes significantly from small changes in body position (e.g. scapula), the intrinsic scanning technique is more appropriate.

3.2. Friction results

Fig. 4a is an example of the force correction for a sliding trial on the leg of the MT. Individual force vectors are plotted with corresponding adjusted force vectors. Fig. 4b displays the displacement of the probe tip during the contact in the motion capture world frame. The probe tip travels along the x-axis, down, then up the z-axis, and does not deviate far from the y-axis of the world frame. Note that the coronal plane of the MT is approximately perpendicular to the z-axis of the world frame. Therefore, the Δz is a reasonable representation of the concave curve of the leg measurement location.

The magnitudes of f_x and f_y increase as the probe tip moves across the measurement target. After the correction, f_x^{adj} and f_y^{adj} are less variable. As the probe tip moves down the slope of the measurement location at the beginning of the touch, the magnitude of f_x and f_y are almost equal to or smaller than the corrected f_x^{adj} and f_y^{adj}. The opposite trend is observed as the probe tip begins to travel up the slope of the measurement location. f_z^{adj} is slightly smaller than f_z as it moves down the curve and larger than f_z as it moves up the curve. These patterns are expected when considering the concave shape of the measurement area. Fig. 4a shows the importance of considering all of the force vectors for a friction measurement on a complicated curve, such as Fig. 2b. In previous work, Wyder-Hodge et al. [15] measured

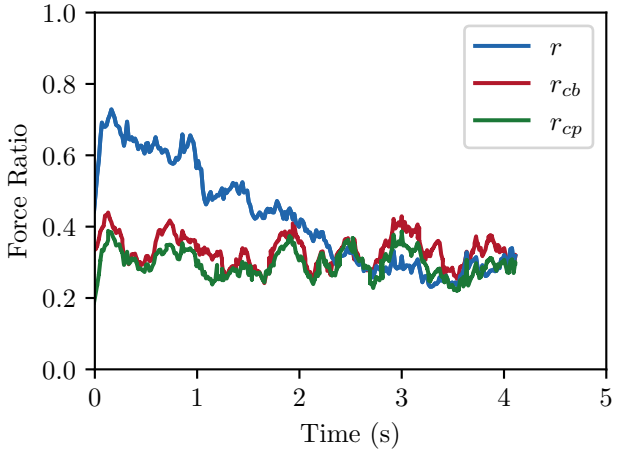

(a) Abdomen

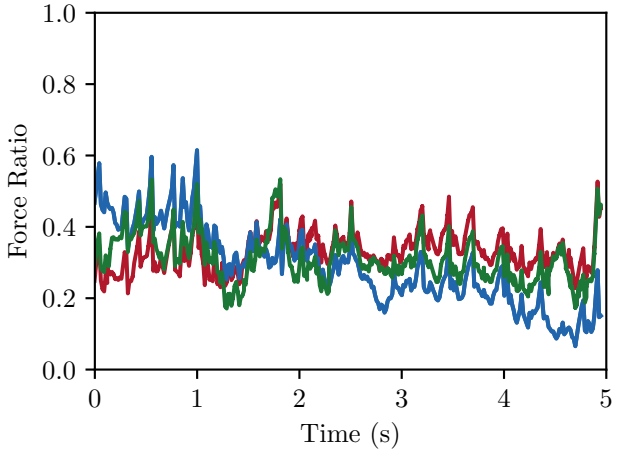

(b) Back

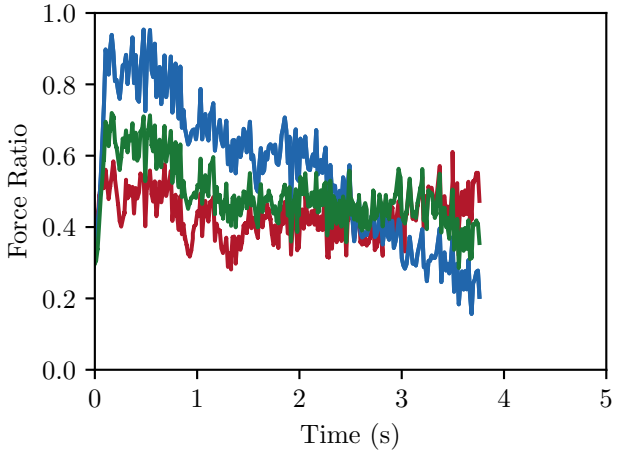

(c) Leg

Figure 6: Displays the r, r_{cb}, and r_{cp} measured on the HT at the three measurement locations: abdomen, back, and leg.

simple structures curved in 2D and implemented the surface correction in 2D. Here, the experimenter attempted to move the probe along the direction of f_x, however, due to the irregularity of the measurement surface and human error, as the experimenter began to move the probe across the surface, the magnitude of f_y grew to make f_y^{adj} a significant component of f_T.

Fig. 5 shows the r, r_{cp}, and r_{cb} of single sliding trials for both locations and all the material conditions on the MT. Table 1 displays the summary statistics for all of the sliding trials on the MT. In Fig. 5a and Fig. 5c the surface mesh used for the surface correction is from the extrinsic scanner. Fig. 5b and Fig. 5d show the correction using the mesh from the intrinsic scanning technique. The back measurement location has a convex shape (Fig. 5a and Fig. 5b), therefore, r decreases because f_{xy} decreases and f_z increases throughout the contact. This is a previously observed trend for convex surfaces [15]. The leg target location (Fig. 5c and Fig. 5d) is concave and we see the opposite pattern than the convex shape in the r traces. The results from the force correction behave as expected, creating less variability in the r_{cp} and r_{cb} than r (see Table 1).

The material surface conditions show three distinct results for the mean force ratios. The silicone surface produces the largest force ratios, the polystyrene produces the next largest, and the lycra surface produces the smallest force ratios. It is expected that the values of each corresponding mean r_{cp} and r_{cb} at the back and leg measurement locations will be approximately the same value due to the same surface making contact. Table 1 shows a r smaller than the r_{cp} and r_{cb} for the back location and r larger than the r_{cp} and r_{cb} for the the leg location (excluding r_{cb} for the polystyrene condition). However, there still exist some differences between the r_{cp} and r_{cb} at the corresponding surface conditions. The trend is consistent for each of the surface conditions, where the mean r_{cp} and r_{cb} are lower at the back location than the leg location. One explanation for this difference may be the variability in sliding velocities between the two measurement locations. At the leg, the mean sliding velocity was 1.6 cm/s, whereas at the back it was 0.9 cm/s. It has been shown that for hard surfaces contacting soft surfaces that velocity may be positively correlated with friction [20, 21, 22]. The difference in the time of the signals plotted in Fig. 5 (and Fig. 6) can be attributed to the variability in the velocity.

The r is the same sliding trial for the extrinsic scan and intrinsic scan conditions in Fig. 5. Therefore, the differences in the r_{cp} and r_{cp} are exclusively due to the different surface meshes. It is evident that the traces are similar, but not the same. This is expected, as each of the surfaces produced from each scanning technique are similar, but have different shapes at a smaller scale, causing different r_c values at the same timestamp. This observation highlights two important factors in this pipeline

- the force measurements are dependent on the shape of the generated surface mesh, and
- an accurate surface mesh will generate more accurate results.

Comparing each of the surface conditions, r, r_{cb}, and r_{cp} for the silicone surface have more fluctuations than for the lycra or the polystyrene condition. This suggests that during the contact on the silicone surface, there is more stick-slip

		Silicone			Polystyrene			Lycra		
		r	r_{cb}	r_{cp}	r	r_{cb}	r_{cp}	r	r_{cb}	r_{cp}
Back	mean	0.762	0.838	0.790	0.445	0.506	0.533	0.066	0.173	0.153
	std	0.261	0.114	0.125	0.226	0.061	0.093	0.136	0.048	0.059
	min	0.246	0.533	0.450	-0.043	0.355	0.335	-0.173	0.024	0.003
	max	1.432	1.280	1.333	1.123	0.894	1.029	0.400	0.295	0.348
Leg	mean	1.169	0.944	0.889	0.649	0.656	0.752	0.329	0.231	0.372
	std	0.348	0.126	0.134	0.179	0.062	0.110	0.128	0.050	0.092
	min	0.432	0.496	0.367	0.216	0.473	0.348	0.045	0.057	0.146
	max	2.154	1.547	1.439	1.037	0.846	1.277	0.582	0.374	0.614

Table 1
Displays the summary statistics for all the sliding trials on the mannequin measurement target. This includes the back and leg locations, the three material conditions, and the three force ratios.

	Back			Leg			Abdomen		
	r	r_{cb}	r_{cp}	r	r_{cb}	r_{cp}	r	r_{cb}	r_{cp}
mean	0.339	0.358	0.338	0.539	0.439	0.516	0.328	0.308	0.325
std	0.116	0.068	0.071	0.163	0.068	0.084	0.114	0.063	0.048
min	0.065	0.204	0.171	0.148	0.257	0.313	0.122	0.144	0.213
max	0.664	0.644	0.599	0.970	0.686	0.885	0.659	0.601	0.562

Table 2
Displays the summary statistics for all the sliding trials on the human measurement target. This includes the back, leg, and abdomen locations, the three material conditions, and the three force ratios.

that is occurring during the contact than on the other two surfaces. The material properties of the silicone may make it harder for the probe to move smoothly across the surface, creating an intermittent or oscillating sliding motion.

Fig. 6 and Table 2 display the results from the sliding trials on the HT. Fig. 6 displays single sliding trials from each of the measurement locations: back, leg, and abdomen. The force ratio corrections are again behaving as expected, where the r_{cb} and r_{cp} are less variable than r. However, there are differences between r_{cp} and r_{cb}, due to the differences in the surface shape of the generated meshes, as mentioned above. All of the measurement locations measured on the human target are convex in shape but have varying curvature. The leg measurement surface features a larger curvature, which results in a larger slope and differences in the minimum and maximum r (Fig. 6c) compared to the other measurement surfaces on the HT (see Table 2). Within the single HT, the mean r_{cp} and r_{cb} measured are the highest at the leg and lowest at the abdomen. However, future work with a large participant pool is needed before making conclusions about differences in sliding skin friction between anatomical regions.

Generally, the mean values of r, r_{cp}, and r_{cb} are similar for the same measurement location. This is likely due to the symmetry of the curves that are measured and the symmetric movement of the probe by the experimenter. If the angle of the probe relative to the measurement surface is similar at a similar displacement from the curve's apex while ascending and descending, then the r mean is likely to be close to the means of the r_{cp} and r_{cb}.

Another source of error in measuring friction on curved surfaces using a handheld device is the researcher's ability to maintain a more uniform f_N during contact. This is important because the COF on surfaces such as human skin has been shown to be dependent on the normal force [23, 9]. The correction proposed here will help with better estimation of the f_T and f_N forces, however, this does not imply that these forces will be consistent throughout the touch.

This is a limitation of a human experimenter operating the tribometer. In the current measurement pipeline, force correction is performed offline after all the data has been collected. However, if the force correction was processed in real-time during the contact, then feedback could be supplied to the experimenter to help maintain a set f_N.

4. Conclusion

In this paper, a method is presented for estimating normal and tangential forces on curved surfaces in 3D with a portable handheld tribometer. Two strategies for generating 3D surface meshes of the measurement surfaces are implemented and compared. The extrinsic scanning strategy may be more accurate and efficient, however, the intrinsic scanning strategy reduces potential error caused by movement between the surface shape measurement and friction measurement. Nevertheless, both strategies successfully reduced the variability of the force ratios measured. This improvement of the force ratio estimation was demonstrated on

irregular concave and convex surface shapes on a mannequin measurement target and three discrete anatomical locations on a human participant.

Acknowledgements

This work was supported, in part, by NSERC Discovery (GR010268), NSERC RTI (GRO19523), and the Canada Foundation for Innovation (LEF20419) grants.

References

[1] A. R. Gwosdow, J. C. Stevens, L. G. Berglund, J. A. Stolwijk, Skin friction and fabric sensations in neutral and warm environments, Textile Research Journal 56 (1986) 574–580. doi:10.1177/004051758605600909.

[2] E. Bertaux, M. Lewandowski, S. Derler, Relationship between friction and tactile properties for woven and knitted fabrics, Textile Research Journal 77 (2007) 387–396. URL: www.trj.sagepub.comhttp://trj.sagepub.com. doi:10.1177/0040517507074165.

[3] A. Ramalho, P. Szekeres, E. Fernandes, Friction and tactile perception of textile fabrics, Tribology International 63 (2013) 29–33. URL: https://www.sciencedirect.com/science/article/pii/S0301679X12002903?via%3Dihub. doi:10.1016/J.TRIBOINT.2012.08.018.

[4] L. Yin, E. Shim, E. DenHartog, A study of skin physiology, sensation and friction of nonwoven fabrics used in absorbent hygiene products in neutral and warm environments, Biotribology 24 (2020) 1–12. doi:10.1016/j.biotri.2020.100149.

[5] M. Temel, A. A. Johnson, A. B. Lloyd, Evaluating the repeatability of friction coefficient measurements and tactile perceptions in skin–textile interactions across body regions, Tribology Letters 70 (2022) 1–12. URL: https://link.springer.com/article/10.1007/s11249-021-01560-5. doi:10.1007/S11249-021-01560-5/FIGURES/7.

[6] Y. Dong, J. Kong, C. Mu, C. Zhao, N. L. Thomas, X. Lu, Materials design towards sport textiles with low-friction and moisture-wicking dual functions, Materials & Design 88 (2015) 82–87. URL: https://www.sciencedirect.com/science/article/pii/S0264127515303567. doi:10.1016/J.MATDES.2015.08.107.

[7] M. J. MacFarlane, P. Theobald, Skin tribology in sport, Biosurface and Biotribology 7 (2021) 113–118. URL: https://ietresearch.onlinelibrary.wiley.com/doi/10.1049/bsb2.12015. doi:10.1049/BSB2.12015.

[8] R. D. Jobanputra, J. Hayes, S. Royyuru, M. A. Masen, A numerical analysis of skin–PPE interaction to prevent facial tissue injury, Scientific Reports 11 (2021) 1–10. URL: https://www.nature.com/articles/s41598-021-95861-3. doi:10.1038/s41598-021-95861-3.

[9] S. Derler, L.-C. Gerhardt, Tribology of skin: review and analysis of experimental results for the friction coefficient of human skin, Tribology Letters 45 (2012) 1–27. URL: http://link.springer.com/10.1007/s11249-011-9854-y. doi:10.1007/s11249-011-9854-y.

[10] A. B. Cua, K. P. Wilhelm, H. I. Maibach, Frictional properties of human skin: relation to age, sex and anatomical region, stratum corneum hydration and transepidermal water loss, British Journal of Dermatology 123 (1990) 473–479. URL: http://doi.wiley.com/10.1111/j.1365-2133.1990.tb01452.x. doi:10.1111/j.1365-2133.1990.tb01452.x.

[11] C. P. Hendriks, S. E. Franklin, Influence of surface roughness, material and climate conditions on the friction of human skin, Tribology Letters 37 (2010) 361–373. URL: http://link.springer.com/10.1007/s11249-009-9530-7. doi:10.1007/s11249-009-9530-7.

[12] P. Eisner, D. Wilhelm, H. I. Maibach, Frictional properties of human forearm and vulvar skin: influence of age and correlation with transepidermal water loss and capacitance, Dermatology 181 (1990) 88–91. URL: https://www.karger.com/Article/FullText/247892. doi:10.1159/000247892.

[13] Y. H. Zhu, S. P. Song, W. Luo, P. M. Elias, M. Q. Man, Characterization of skin friction coefficient, and relationship to stratum corneum hydration in a normal Chinese population, Skin Pharmacology and Physiology 24 (2011) 81–86. URL: /pmc/articles/PMC2997446//pmc/articles/PMC2997446/?report=abstracthttps://www.ncbi.nlm.nih.gov/pmc/articles/PMC2997446/. doi:10.1159/000321993.

[14] L. Vilhena, A. Ramalho, Friction of human skin against different fabrics for medical use, Lubricants 4 (2016) 1–10. URL: http://www.mdpi.com/2075-4442/4/1/6. doi:10.3390/lubricants4010006.

[15] P. A. Wyder-Hodge, E. Larionov, D. K. Pai, In situ measurement of friction on curved surfaces, Tribology International 173 (2022) 1–9. doi:10.1016/j.triboint.2022.107591.

[16] D. K. Pai, A. Rothwell, P. Wyder-Hodge, A. Wick, Y. Fan, E. Larionov, D. Harrison, D. Raj Neog, C. Shing, The human touch: measuring contact with real human soft tissues, ACM Trans. Graph 37 (2018) 1–12. URL: https://doi.org/10.1145/3197517.3201296. doi:10.1145/3197517.3201296.

[17] M. Kazhdan, M. Bolitho, H. Hoppe, Poisson surface reconstruction, in: Eurographics Symposium on Geometry Processing, 2006, pp. 1–10. URL: https://www.cse.iitd.ac.in/~mcs112609/poission.pdf.

[18] Q.-Y. Zhou, J. Park, V. Koltun, Open3D: a modern library for 3D data processing, 2018. URL: https://arxiv.org/abs/1801.09847v1. doi:10.48550/arxiv.1801.09847.

[19] A. Jacobson, D. Panozzo, others, {libigl}: A simple {C++} geometry processing library, 2018. URL: https://libigl.github.io/.

[20] S. S. Ramkumar, A. S. Umrani, D. C. Shelly, R. W. Tock, S. Parameswaran, M. L. Smith, Study of the effect of sliding velocity on the frictional properties of nonwoven fabric substrates, Wear 256 (2004) 221–225. doi:10.1016/S0043-1648(03)00440-X.

[21] R. Cross, Increase in friction force with sliding speed, American Journal of Physics 73 (2005) 812–816. doi:10.1119/1.1891174.

[22] P. Sadowski, S. Stupkiewicz, Friction in lubricated soft-on-hard, hard-on-soft and soft-on-soft sliding contacts, Tribology International 129 (2019) 246–256. doi:10.1016/J.TRIBOINT.2018.08.025.

[23] M. J. Adams, B. J. Briscoe, S. A. Johnson, Friction and lubrication of human skin, Tribology Letters 26 (2007) 239–253. URL: http://link.springer.com/10.1007/s11249-007-9206-0. doi:10.1007/s11249-007-9206-0.